ISBN: 978-3-95450-249-3 ISSN: 2673-5350 doi: 10.18429/JACoW-IBIC2024-TUP46

DESIGN AND DEPLOYMENT OF AN IN-VACUUM ELECTRO-OPTIC BPM AT THE CERN SPS

M.Z.C. Bosman*, S.M. Gibson, D.M. Harryman, A. Arteche
John Adams Institute at Royal Holloway, University of London, UK
T. Lefèvre, T.E. Levens, CERN, Geneva, Switzerland

Abstract

The Electro-Optic Beam Position Monitor employs electro-optically active Lithium Niobate crystals with fibre-coupled laser interferometry to measure the propagating electric field from passing proton bunches in the Super Proton Synchrotron to infer their position and intra-bunch instabilities. A feedback algorithm continually adjusts the laser wavelength, and thereby the phase offset, so the interferometric bias point is kept in the linear range. Tests to validate the EO-BPM were conducted with comparison to current technology. Results show that the EO-BPM can identify turn-by-turn oscillations and its optical centre is offset from the beam pipe centre.

INTRODUCTION

The High-Luminosity Large Hadron Collider (HL-LHC) project at CERN aims to significantly increase the luminosity of the LHC and allow for more data to be collected by the LHC experiments. Part of the luminosity increase will be achieved by installing crab cavities to induce a transverse displacement within the proton bunches in order to improve the overlap of the colliding bunches in the interaction point [1].

An Electro-Optic Beam Position Monitor (EO-BPM) is being developed as a high-bandwidth (at least 4 GHz) diagnostic tool for crabbing and intra-bunch instability detection at HL-LHC. The EO-BPM senses the propagating electric field, induced by the passing proton bunch, using electro-optic crystals [2].

Following previous tests of an in-air design in HiRadMat [3], an ultra-high vacuum compatible device has recently been installed in the Super Proton Synchrotron (SPS) as a proof of concept of the HL-LHC design.

WORKING PRINCIPLE

Background

Some electro-optically active crystals incur a change in refractive index that is linear with the electric field induced in the crystal. This is known as the Pockels effect [4].

Lithium niobate (LNB) is an electro-optical birefringent crystal [5]. This means that the refractive index of one of its three principal axes differs from the other two. Due to the Pockels effect, this difference between the two refractive indices can be further enhanced by applying an external electric field to the crystal. Using linearly polarised laser light, this change due to the external field can be measured using interferometry. In such a way the external field, which in our case resembles the bunch shape, can be inferred [2].

EO Button Design

To focus the beam's electric field inside the crystal, a 9 mm diameter, electrically floating, electrode is placed in contact with the LNB crystal (shown in Fig. 1) [6]. The electric field induced by the bunch is focused by this bottom electrode and projected into the LNB crystal and via the top electrode to a termination on top.

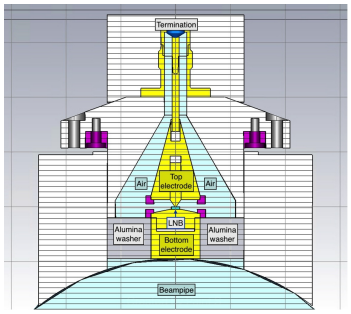

Figure 1: Transverse profile slice of 3D render EO-BPM, showing the beam pipe, floating electrode connected to LNB crystal and the top electrode.

Another method used to enhance the electric field in the crystal is the use of a waveguide. Narrowing the crystal to a 10 μm waveguide significantly concentrates the projected electric field from the bottom electrode. The fibre-coupled laser is attached to the narrowest part to maximise effectiveness [3].

A fibre-coupled laser is split and passes through two waveguides placed on opposite sides of the beam pipe. The outputs are then recombined to act as a Mach-Zehnder (MZ) interferometer (see Fig. 2) with two outputs in antiphase (C+, C-). The fibres are connected to the waveguide perpendicular to the profile in Fig. 1.

Output

The output of this interferometer is of the form

$$V = A + B\,cos(\phi_0 + \pi\frac{\Delta E_c}{E_\pi}), \tag{1}$$

and the normalised transfer function is

$$T_{inter} = \frac{1}{2} + \frac{1}{2}\,cos(\phi_0 + \pi\frac{\Delta E_c}{E_\pi}), \tag{2}$$

where ϕ_0 is defined as the phase offset, ΔE_c the difference in electric field in both waveguides, and E_π the electric field required for a phase advance of π.

* max.bosman@rhul.ac.uk

ISBN: 978-3-95450-249-3 ISSN: 2673-5350 doi: 10.18429/JACoW-IBIC2024-TUP46

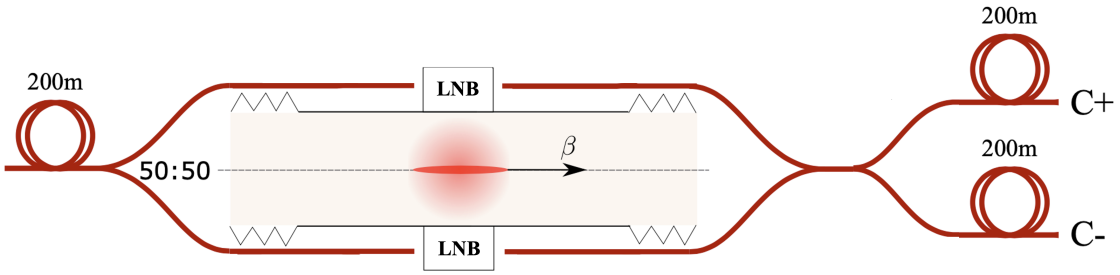

Figure 2: Diagram of EO-BPM splitter tree; laser travels from left to right, splits and passes through opposite crystals, then recombines and splits to give two interferometric signal outputs in anti-phase.

VACUUM DESIGN & ASSEMBLY

The EO-BPM has a 285 mm long ultra-high vacuum compatible 316LN stainless steel body with 80 mm internal diameter and DN100 flanges. The body dimensions were chosen to match an existing LHC BPM type and allow its support design and integration to be reused.

An alumina ceramic washer (relative permittivity: ε_r = 9.9) is used to form the vacuum seal between the body and the central electrode. This washer is brazed to both the central electrode and an outer ring made of Kovar, chosen to match the thermal expansion coefficient of the ceramic. Otherwise, the difference in thermal expansion and brittleness of the alumina pose a risk of cracking during brazing. The outer ring is then electron beam welded into the body. Figure 3a shows the washer in the body after brazing and welding.

The EO button assembly consists of the waveguide placed between copper top and bottom electrodes in its housing. The housing and electrodes form a 50 Ω coaxial line which is terminated by an external 50 Ω termination to minimise reflections. The buttons have been designed as a separate sub-assembly to allow removal during the bake-out procedure which is required to achieve the LHC ultra-high vacuum conditions. A good electrical contact with the central electrode and body is assured with spring contacts, as shown in Fig. 3b. The spring contacts of the bottom copper piece, formed by electrical discharge machining, fit into a recess in the brazed central electrode. The complete assembly is shown in Fig. 3c where the blue fibres for the laser input and output can be seen as well as the external 50 Ω termination.

Two EO button assemblies were built in the lab and mounted on the EO-BPM body before it was transported to the SPS. The optical splitter tree, positioned on top of the body, was also assembled in the lab. The left crystal has an optical power loss of 5.2 dB and the right crystal a power loss of 7.0 dB due to imperfect connections of the fibres to the 10 μm waveguide.

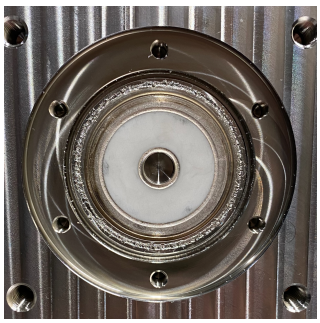

(a) Ceramic washer brazed into the EO-BPM body

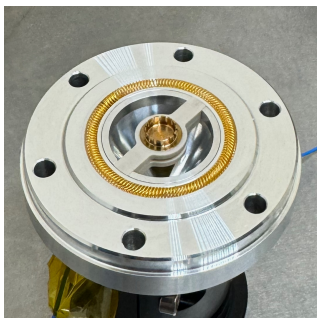

(b) EO-BPM button assembly, mating view

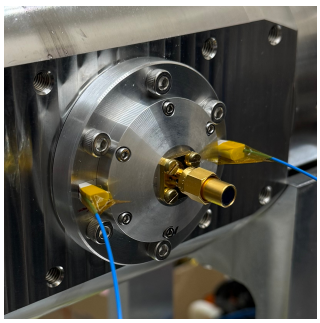

(c) EO-BPM button assembled onto the body

Figure 3: Photos showing detail of the ceramic washer brazed to the EO-BPM body, mating interface to the button assembly and button assembled onto the body.

SPS INSTALLATION

The EO-BPM was successfully installed in the SPS ring during the year-end technical stop in January 2024. Figure 4 shows the EO-BPM installed on its alignment platform in the SPS tunnel. Specific upstream and downstream transition chambers were designed to adapt the 285 mm long

ISBN: 978-3-95450-249-3 ISSN: 2673-5350 doi: 10.18429/JACoW-IBIC2024-TUP46

EO-BPM to the 502 mm available space and to the 83 mm internal diameter beam pipe with conical flanges used on the neighbouring equipment.

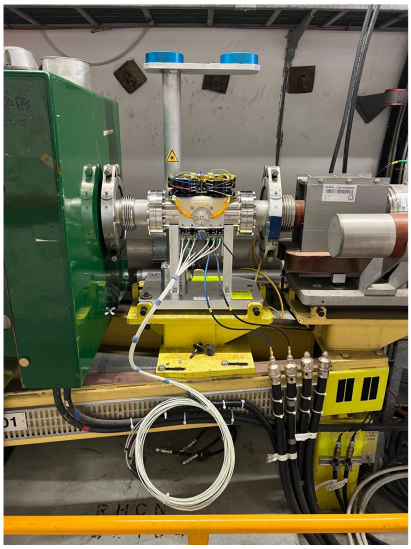

Figure 4: EO-BPM installed in the SPS on its alignment platform. The beam propagates from left to right.

In a radiation-free zone, some 200 m from the SPS tunnel, a 780 nm continuous-wave (CW) laser (TLB 6800 Vortex Plus) with a tunable wavelength and an optical power of 30 mW is amplified to 100 mW by an optical amplifier (Toptica BoosTA Pro). The amplified laser output is connected to a polarisation-maintaining (PM) fibre to the SPS tunnel which was installed for the initial EO-BPM tests [7] and has been reused for this new installation. The laser passes through the EO-BPM (see Fig. 2) and the output signals are routed back to the same radiation-free zone by additional long single-mode (SM) fibres.

The EO-BPM interferometric output ranges from 0.2 mW to 4.1 mW, corresponding to an average power transfer of 2.1%. The loss in power is due to the use of several splitters, as well as losses in the waveguides, losses in the long fibres and insertion losses of the fibre connectors.

The interferometric output signal is connected to an amplified photodetector (Thorlabs RXM10CF, bandwidth: 10 GHz), which converts the optical signal to a voltage. This signal is digitised using an oscilloscope (Keysight DSOS404A, bandwidth: 4 GHz, sampling rate: 10 Gsps). The photodetector contributes an RMS noise level of 0.46 mV and the scope has a RMS noise level of 1.6 mV (at 100 mV/div). Collectively, the detector chain contributes a RMS noise level of 1.7 mV.

RESULTS

Drift Control

It has been found that the interferometric working point of the EO-BPM drifts randomly, even in the absence of an external electric field, at a rate of <1 rad/s. The exact source has not been identified, but it is thought that this could be due to temperature variations affecting the interferometer arm length, charge buildup on the buttons or mechanical vibrations.

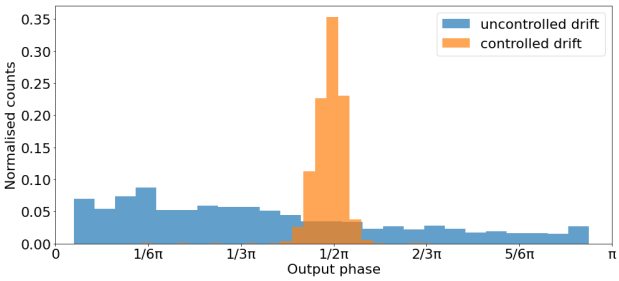

Figure 5: Histogram showing phase offset for controlled and uncontrolled drift, bin size is $\frac{\pi}{25}$.

In order to keep the working point in the linear range of the transfer function, it is important that the phase offset is kept consistent and close to $\frac{\pi}{2}$. To achieve this, the laser wavelength is continuously adjusted to keep a phase offset of $\frac{\pi}{2}$ within a small margin.

To control the working point, a simple feedback algorithm has been implemented in Python. One of the two interferometer outputs is used to measure the difference from a reference value, namely the average voltage output of the digitised signal. The algorithm then adjusts the laser wavelength by a value proportional to this difference. This adjustment occurs at a frequency of 5 Hz and results in the phase offset being kept close to $\frac{\pi}{2}$ as shown in Fig. 5 where the histogram of the phase offset for both a controlled and an uncontrolled case are shown.

Signal Comparison

The EO-BPM has been shown to successfully record intra-bunch turn-by-turn data. These results can be compared with the existing technology, namely the Head-Tail Monitor (HT) located 18 m downstream.

The HT employs 600 mm long stripline electrodes on opposing sides of the beam pipe. These electrodes act as directional couplers and gain a pulse charge from the passing beam. A passive 180° hybrid (Macom H-9) is used to calculate difference and sum signals from opposing electrodes which are digitised after 150 m of 7/8" coaxial cable using the same type of oscilloscope that is used for the EO-BPM [8].

Figure 6 shows 10 overlaid turns of a single LHC type bunch (4σ = 2.70 ns, 2.2E11 protons) at injection. The first to last turns are represented by the colour of the traces, from blue to red respectively. The same turns are shown for both the EO-BPM (Fig. 6a) and for the HT difference (Fig. 6b) and sum (Fig. 6c) signals. The signals have been normalised to the peak of the average of all turn. Two different effects, due to the injection, are visible in the data. A change of the longitudinal bunch shape after injection is evident in the HT sum signal where the bunch peak can be seen to increase as the bunch length shortens. In addition, transverse injection

ISBN: 978-3-95450-249-3 ISSN: 2673-5350 doi: 10.18429/JACoW-IBIC2024-TUP46

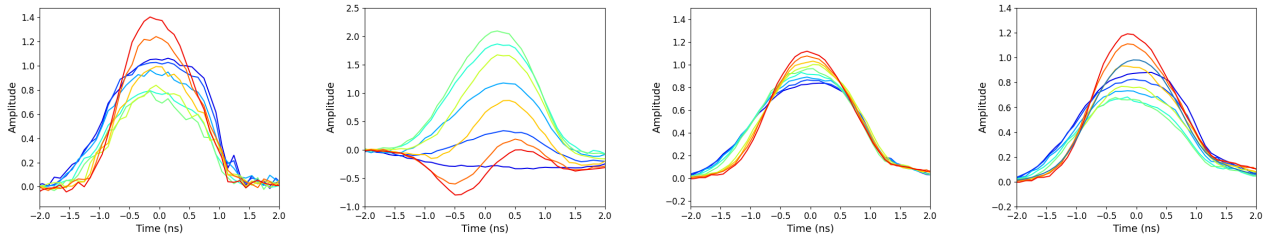

(a) EO-BPM (b) HT difference (c) HT sum (d) Combined HT sum & diff.

Figure 6: Turn-by-turn signals from 10 turns of a 2.2E11 proton bunch at injection to the SPS, as measured by the EO-BPM and the Head-Tail Monitor (HT). The signals have been normalised to the peak of the average of all turns. Blue represents the first turn and red represents the last turn.

oscillations from turn-to-turn are visible in the HT difference signal.

Figure 6d shows a combination of the HT signals where the difference signal has been scaled empirically by a factor of 0.15 and subtracted from the sum signal. Visual comparison with the EO-BPM signal shows clear similarities and implies that the EO-BPM bears characteristics of both of the HT signals: transverse oscillations, akin to the difference signal, which are superimposed on an overall bunch shape similar to the sum signal.

If the optical centre of the EO-BPM was exactly centred on the beam pipe, its signal should more closely resemble the difference signal without the longitudinal bunch shape component. Preliminary analysis of the data shows that the EO-BPM signal resembles a signal for an optical centre deviation of approximately 10 mm in the direction of the left button. As the beam position is inferred from the difference in electric field in the crystals (Eq. (1)), this implies that the opposing buttons somewhat differ in their response to the electric field from the beam. More analysis into its cause and solution is required.

The bunch length, calculated by fitting a Gaussian to the average of the traces, from the HT is $4\sigma = 2.83$ ns while from the EO-BPM is $4\sigma = 2.70$ ns, about a 5% difference.

The signal-to-noise ratio (SNR) is calculated by first subtracting the average of the traces in Fig. 6 to isolate only the oscillation component. Then a 3 ns window around the bunch peak is taken as the signal and a 3 ns window outside the bunch as the noise. From this analysis, the SNR for the EO-BPM signal is 19.8 dB, compared to 33.4 dB for the HT difference signal. As the SNR of the EO-BPM is dominated by the noise of the photodetector and oscilloscope, this is only valid for these bunch intensities and the SNR will be worse at lower bunch intensities. Due to the mismatch between the buttons, a large part of the oscilloscope's dynamic range must be used for digitising the unwanted longitudinal component. Therefore, one avenue to improve the SNR of the EO-BPM is to improve the matching of the buttons. This will allow further pre-amplification of the transverse signal to better use the available dynamic range of the digitizer.

CONCLUSION AND OUTLOOK

The Electro-Optic Beam Position Monitor (EO-BPM) is a state-of-the-art technology that is being developed as a diagnostic tool for crabbing and intra-bunch instability detection in HL-LHC. It uses electro-optically active lithium niobate crystals in a Mach-Zehnder interferometer to detect the displacement of a passing proton bunch with high bandwidth.

Following in air tests at HiRadMat, an ultra-high vacuum compatible prototype has recently been installed in the SPS and can be directly compared to the stripline Head-Tail Monitor (HT) that is currently used for intra-bunch diagnostics.

An initial comparison of the turn-by-turn data from both instruments shows that the EO-BPM bears characteristics of both the HT sum and difference signal. From the presented data it can be seen that the longitudinal bunch shape, as well as transverse oscillations, are both visible. Ideally, the EO-BPM should give a purely transverse signal without the longitudinal component. The optical centre of the installed EO-BPM has been shown to be approximately 10 mm offset from the beam pipe centre. This is thought to be due to the different response of the installed buttons to the beam field. Furthermore, the EO-BPM detection chain generates more noise than the Head-Tail Monitor, resulting in a lower SNR of 19.8 dB, compared to 33.4 dB, for the presented data.

Ways of improving the matching between the buttons, and the overall SNR of the instrument, are currently being investigated. A more quantitative comparison of the data will be presented in the future.

ACKNOWLEDGEMENTS

We would like to thank Nicolas Chritin and the EN-MME team for the design of the EO-BPM vacuum body and Fritz Motschmann for his help with brazing at CERN.

Work supported by UK STFC grants ST/N001583/1, ST/P00203X/1, Royal Holloway Univ. of London & CERN.

REFERENCES

[1] O. Aberle *et al.*, "High-Luminosity Large Hadron Collider (HL-LHC): Technical design report", Tech. Rep. CERN-2020-010, 2020. doi:10.23731/CYRM-2020-0010

ISBN: 978-3-95450-249-3 ISSN: 2673-5350 doi: 10.18429/JACoW-IBIC2024-TUP46

[2] S. M. Gibson *et al.*, "High Frequency Electro-Optic Beam Position Monitors for Intra-Bunch Diagnostics at the LHC", in *Proc. IBIC'15*, Melbourne, Australia, Sep. 2015, pp. 606–610. doi:10.18429/JACoW-IBIC2015-WEDLA02

[3] S. M. Gibson *et al.*, "Electro-Optical BPM Development for High Luminosity LHC", in *Proc. IBIC'22*, Kraków, Poland, pp. 181–185, 2022. doi:10.18429/JACoW-IBIC2022-TU1I1

[4] C. Peucheret, "Elements of Electromagnetic Theory, Anisotropic Media, and Light Modulation by the Linear Electro-Optic Effect", *Physics*, no. 12421920, 2010.

[5] R. S. Weis and T. K. Gaylord, "Lithium niobate: Summary of physical properties and crystal structure", *Appl. Phys. A*, vol. 37, no. 4, pp. 191–203, 1985. doi:10.1007/BF00614817

[6] A. Arteche *et al.*, "Beam Measurements at the CERN SPS Using Interferometric Electro-Optic Pickups", in *Proc. IBIC'19*, Malmö, Sweden, Sep. 2019, pp. 457–460. doi:10.18429/JACoW-IBIC2019-WEAO04

[7] A. Arteche *et al.*, "First Beam Tests at the CERN SPS of an Electro-Optic Beam Position Monitor for the HL-LHC", in *Proc. IBIC'17*, Grand Rapids, MI, USA, Aug. 2017, pp. 270–273. doi:10.18429/JACoW-IBIC2017-TUPCF23

[8] T. E. Levens *et al.*, "Automatic detection of transverse beam instabilities in the Large Hadron Collider", *Phys. Rev. Accel. Beams*, vol. 22, no. 11, p. 112 803, 2019. doi:10.1103/PhysRevAccelBeams.22.112803